Journal of Alloys and Compounds 504 (2010) 440–445

Contents lists available at ScienceDirect

Journal of Alloys and Compounds

journal homepage: www.elsevier.com/locate/jallcom

Correlation between structural and electrical properties of $Mg_{1-2x}Zn_xNi_xAl_2O_4$ ($x = 0.0–0.5$) ceramic nanomaterials synthesized by a urea assisted microwave combustion method

Muhammad Javed Iqbal*, Bushra Ismail

Surface and Solid State Chemistry Laboratory, Department of Chemistry, Quaid-i-Azam University, Islamabad 45320, Pakistan

ARTICLE INFO

Article history:
Received 26 September 2009
Received in revised form 19 May 2010
Accepted 29 May 2010
Available online 11 June 2010

Keywords:
Nanostructured materials
Ceramics
Semiconductors
X-ray diffraction
Scanning electron microscopy

ABSTRACT

A urea assisted microwave combustion method was used to synthesize $Mg_{1-2x}Ni_xZn_xAl_2O_4$ ($x = 0.0–0.5$) ceramic materials. X-ray diffraction (XRD) analysis confirmed the formation of a single spinel phase with an average Scherrer crystallite size of in the range 24–51 nm. The chemical composition of the synthesized compounds was determined by energy dispersive X-ray fluorescence (ED-XRF). The synthesized materials show crystalline morphology as evidenced by scanning electron microscopy (SEM) and transmission electron microscopy (TEM) results. Spinel formation was confirmed by the appearance of peaks at 550 and 712 cm^{-1} in the FTIR spectra. A significant increase in room the temperature (RT) resistivity from 0.27×10^9 to 9.41×10^9 Ω cm was achieved by doping with a binary mixture of Ni–Zn. The dielectric constant (ε) and the loss tangent ($\tan\delta$) follow the mechanism of space charge polarization. High resistivity, a low dielectric constant and a small loss tangent make the materials suitable for applications as insulators and electromagnetic radiation absorbers in the electronics industry.

1. Introduction

Magnesium aluminum spinel (MAS) $(Mg^{2+})[Al^{3+}, Al^{3+}]O_4$ is a normal spinel in which the divalent Mg^{2+} ions occupy tetrahedral sites, represented by parenthesis, and the trivalent Al^{3+} ions occupy octahedral sites, represented by square brackets. It has a high melting point (~2400 K), low density (3.58 g/cm^3), excellent strength at extremely high temperatures, good resistance against chemical attacks, optical transmittance in the wavelength region between 0.25 and 5 μm, high electrical resistivity and low dielectric losses [1–3]. These properties allow MAS and related compounds to be used as catalysts or catalyst support materials, humidity sensors, refractories, dielectric capacitors in electronic devices, insulators and electromagnetic radiation absorbers, radiation resistant materials and materials for transparent armors [4,5].

The main focus of the current research activities on MAS spinel is two fold, viz.: improvement of properties by reducing the dimensions down to the nanoscale, hence, introducing many novel synthesis routes and the study of doping effects of various rare earth and transition metals ions, hence, elaborating mechanical, structural, optical and the thermal properties of MAS to be used in the applications mentioned in the first paragraph. We will present a brief literature review on both the aspects of the recent research to update the progress in the current state-of-knowledge on this topic.

The common synthesis methods like hydrothermal techniques, spray pyrolysis, spark plasma synthesis, sol–gel methods, co-precipitation, molten salt synthesis, etc. [6,7], have been used to date which result in the controlled homogeneity and purity, lower annealing temperatures and a better control over the size of the synthesized particles, on the other hand, these methods have not received commercial importance because of the high costs of reagents and the processes involved. Various new methods and the old ones with some modifications have been used for the synthesis of the nanosized materials. These methods include the reverse micelle synthesis [8], microwave assisted hydrothermal method [9], surfactant assisted co-precipitation method [1,6], sonochemical method [10], mechanical activation [3] and a combined gelation and precipitation method [11].

The microwave combustion method has evolved recently [12] and has an advantage over the others in requiring lower reaction times and a uniform heating of the reactants forming homogeneous, high-purity and crystalline powders. The energy consumption is also minimized as opposed to the other methods like sol–gel and co-precipitation in which annealing at the higher temperatures is required for several hours to get a single spinel phase.

Recently, photo-luminescent properties of the transition metals (Co^{2+}, Mn^{2+}, Cr^{3+}) and the rare earth metals (Eu^{2+}, Dy^{3+}, Nd^{3+}, Ti^{3+}, Tb^{3+}) doped aluminates have attracted the attention of researchers

* Corresponding author. Tel.: +92 51 90642143; fax: +92 51 90642241.
E-mail address: mjiqauchem@yahoo.com (M.J. Iqbal).

0925-8388/$ – see front matter © 2010 Elsevier B.V. All rights reserved.
doi:10.1016/j.jallcom.2010.05.142

[13–15] because of their potential use in the picture tubes and the plasma display panels and as phosphors. The lifetime extracted from the decay curve for Dy^{3+} doped $MgAl_2O_4$ was found to be 0.407 ms (λ_{ex} = 258 nm, λ_{em} = 483 nm) and 0.354 ms (λ_{ex} = 380 nm, λ_{em} = 480 nm) [15] while Eu^{3+} doped $MgAl_2O_4$ with high luminous efficiency at 615 nm with 393 nm excitation [14]. Similarly, Cr containing alloys developed for the hydrogen storage exhibit improved electrochemical properties [16]. The microwave dielectric properties of Zn^{2+} substituted MAS have been studied for their applications in resonators, filters, and substrates in the wireless communications [17].

In the past magnesium aluminate was attempted to dope with single ions (Ca^{2+}, Ba^{2+}, Sr^{2+}, Fe^{3+}, Cr^{3+} and Mn^{3+}) and with binary mixtures of Zr/Co and Zr/Ni, and the effects of such substitutions on the structural, electric and dielectric properties were reported [18–20]. The electrical resistivity values of 3.25–6.45 $\times 10^9$ Ω cm and 3.14–6.73 $\times 10^9$ Ω cm and dielectric constant and loss tangent values of 5.80–8.09 and 0.0051–0.11, respectively, have been achieved.

The present study focuses on the synthesis of Ni/Zn double doped magnesium aluminate samples of the general formula $Mg_{1-2x}Zn_xNi_xAl_2O_4$ (x = 0.1–0.5) using cost effective microwave combustion method. Co-doping is carried out to achieve better optimization of electrical resistivity, dielectric constant and dielectric loss values in the samples thus making them suitable as insulators in fusion reactors, dielectric capacitors in electronic devices, and for applications in the electronics industries as insulators and electromagnetic radiation absorbers. The microwave method is employed for the synthesis and urea is used as a combustion aid. A domestic microwave oven was slightly modified to remove any gases produced during different stages of the synthesis. Various physical characteristics of the spinel samples are investigated that include lattice parameter, unit cell volume, theoretical density, crystallite size, temperature variation of resistivity, activation energy, dielectric constant and dielectric loss variations with increasing frequencies.

2. Experimental

Analytical grade chemicals were used as received, namely, $Mg(NO_3)_2{\cdot}6H_2O$ (Merck, 99.9%), $Al(NO_3)_3{\cdot}9H_2O$ (Merck, 95.0%), $Zn(NO_3)_2{\cdot}6H_2O$ (Riedel, 98.0%), $Ni(NO_3)_2{\cdot}6H_2O$ (Riedel, 99.999%) and $(NH_2)_2CO$ (Riedel, 99.5%). Combustion synthesis under microwave irradiation was carried out previously by [12] and Reddy et al. [21] where reaction times of 40–100 min were required. On the contrary, drastically reduced reaction times of approximately 2 min were achieved in the present study by carrying out the reaction of stoichiometric amounts of the metal nitrates together with urea in the aqueous phase.

$Mg(NO_3)_2{\cdot}6H_2O$, $Al(NO_3)_3{\cdot}9H_2O$ and $(NH_2)_2CO$ were weighed in ratios of 1:2:6.67, respectively, and mixed thoroughly in 15 ml of de-ionized water at room temperature to make a clear solution which was then heated for 2 min in a 1500 W domestic microwave oven (General, S/N 441PN90D00) at a microwave frequency of 2.45 GHz. For an efficient removal of the expected gases, like CO_2, H_2O, or N_2 and NO_2, an external exhaust fan was attached at the outlet window. Brown colored fumes were evolved during the initial heating period followed by transparent fumes, and the content of the beaker after the combustion was identified as spinel. The same reaction carried out in the solid state resulted in a non-uniform combustion of the reactants leaving patches of un-reacted nitrates along with the product. Double doped samples were also prepared from aqueous solutions by the described method. An attempt to synthesize the spinel using metal acetates as reactants was not successful.

The samples were characterized by powder X-ray diffractometry (PANalytical model 3040/60 X' Pert PRO) using Cu Kα radiation, and data were collected in the 2θ range from 15° to 80°. Diffraction peaks were used to identify the structure of the samples by matching their observed patterns with the standard pattern of magnesium aluminate spinel (ICSD ref. code No. 00-021-1152, a = 8.08 Å, V_{cell} = 528 Å^3). The microstructure of the synthesized samples was studied using scanning electron microscopy (Hitachi VP-SEM S-3400N). Particles sizes were analyzed by means of a transmission electron microscope (TEM) (Philips CM200). For this purpose, dispersions of the samples in ethyl alcohol were prepared in an ultrasonic bath for 15 min, and a carbon coated TEM grid was dipped into the solution and dried for analysis. Thermal analysis (TGA/DTG) was performed by a thermal analyzer (Mettler-Toledo, TGA/SDTA851e) at heating rates of 5 K/min. The chemical composition of the samples was determined by energy dispersive X-ray fluorescence spectroscopy (ED-XRF, Horiba, MESA-500). The FTIR spectra were recorded in the mid-IR region, i.e. 400–4000 cm^{-1}, using KBr pellets by an Excalibur Bio-Rad (FTS 3000MX) spectrometer.

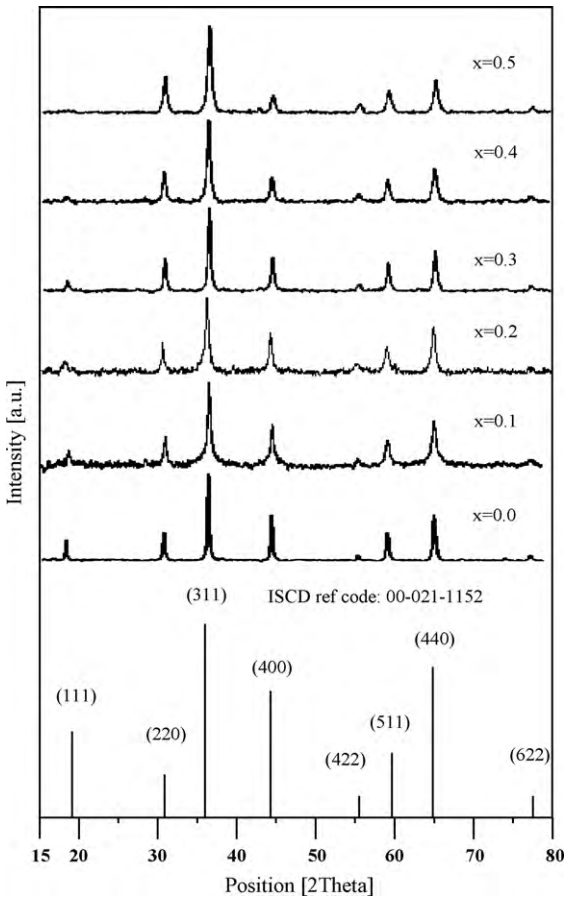

Fig. 1. XRD patterns for $Mg_{1-2x}Zn_xNi_xAl_2O_4$ (x = 0.0–0.5) samples along with the standard pattern of magnesium aluminate.

The DC electrical resistivity was measured in the temperature range of 298–673 K using a laboratory built apparatus to bring two probes in contact with the sample, a method commonly known as two-point probe method, and no preheating of the samples was carried out. One of the probes allowed the DC voltage from a constant voltage source (±0.0001 V) and the other probe employed the source meter (Keithley, Model 2400) to measure the resulting change in current across the surface of samples (±0.0001 μA). A PT100 thermocouple was connected to the temperature sensing multimeter (Uni, UT 55) for temperature measurements (±0.01 K).

The capacitance and the dielectric loss (tan δ) measurements of the samples pressed into pellets were carried out at room temperature in an ac frequency range of 10^3–10^6 Hz using an Inductance Capacitance Resistance (LCR) meter bridge (Wayne Kerr LCR 4275). The surface of the sample pellets was coated by a layer of silver paste (Agar Scientific). The DC electrical resistivity and the dielectric measurements were carried out with sample pellets of 13 mm diameter and 1 mm thickness.

3. Results and discussion

Fig. 1 shows a comparison of the XRD patterns of Ni/Zn double doped samples of the general formula $Mg_{1-2x}Zn_xNi_xAl_2O_4$ (x = 0.1–0.5). Sharp and high intensity peaks are obtained with $h\,k\,l$ values of (1 1 1), (2 2 0), (3 1 1), (4 0 0), (5 1 1) and (4 4 0) which closely correspond to the standard pattern of spinel $MgAl_2O_4$ compound (ICSD ref. code No. 00-021-1152, a = 8.08 Å, V_{cell} = 528 Å^3). The absence of any extra peaks in these patterns indicates that the synthesized samples consist of purely single-phase of MAS [22,23]. The lattice constant (a) was calculated from the X-ray powder diffraction data using following equation [24]:

$$a = d[(h^2 + k^2 + l^2)]^{1/2} \quad (1)$$

where d is the value of the d-spacing of lines in the XRD pattern, $h\,k\,l$ are the corresponding indices of each line in the pattern. The unit cell volume is calculated using $V_{cell} = a^3$.

The crystallite size (D) was calculated using the Debye–Scherrer equation [24]:

$$D = \frac{k\lambda}{\beta \cos\theta_B} \quad (2)$$

where β is the broadening of the diffraction line measured as full width at half maxima (FWHM) which is corrected for instrumental broadening using the relation $\beta = (\beta^2_{\exp} - \beta^2_{inst})^{1/2}$, where β_{exp} is the broadening of the sample, β_{inst} is the broadening for the $MgAl_2O_4$ composed of large particles >500 nm, λ is the X-ray wavelength (1.542 Å), θ the Bragg's angle and k a constant which is equal to 0.9 (for cubic system). The X-ray densities ($d_{X\text{-ray}}$) of all the samples were calculated by the following relation [24]:

$$d_{X\text{-ray}} = \frac{ZM}{V_{cell}N_A} \quad (3)$$

where Z is the number of formula units per unit cell (Z = 8 for the spinel structure), M is the molar mass, V_{cell} and N_A have their usual meanings.

Lattice parameter, a, and cell volume, V_{cell}, of the synthesized samples are in accordance with the values of the standard magnesium aluminate spinel (ICSD ref. code No. 00-021-1152, a = 8.08 Å, V_{cell} = 528 Å^3) indicating that the double doped samples maintain the cubic symmetry of the spinel lattice. The density of the doped samples increases gradually with the increase in dopant content due to the larger molar mass of the double doped samples compared with the undoped magnesium aluminate as the atomic mass of Ni (58.69) and Zn (65.38) is higher than that of Mg (24.31). The crystallite sizes of the samples vary in the range of 24–51 nm.

Energy dispersive X-ray fluorescence (ED-XRF) was employed to determine the chemical composition of the synthesized samples as listed in Table 1. The observed compositions of the synthesized samples agree well with the nominal compositions. Slightly lower values of Zn content in the synthesized samples are due to the loss of some Zn during the synthesis process [25]. A scanning electron microscopic (SEM) image of the magnesium aluminate sample is shown in Fig. 2. The aggregation of crystallites to form large masses of particles may be due to the high temperatures involved in the microwave synthesis. TEM images for magnesium aluminate (a), as well as for doped samples with x = 0.2 (b) and x = 0.4 (c) are shown in Fig. 3. The particle size of the undoped sample is larger and becomes smaller on account of doping. Large agglomerates are formed by the combination of nanosized grains. Selected area diffraction patterns are also shown in the inset of Fig. 3 in the form of fringes

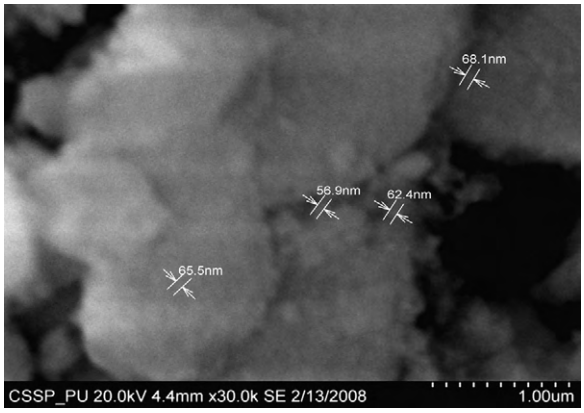

Fig. 2. SEM micrograph for $MgAl_2O_4$ recorded at a magnification of 30,000.

and d-spacings, and hence lattice parameters are also found similar to those calculated on the basis of XRD analysis. TGA/DTG curves for the microwave synthesized $MgAl_2O_4$ and $Mg_{0.2}Zn_{0.4}Ni_{0.4}Al_2O_4$ are shown in Fig. 4(a) and (b), respectively, showing corresponding weight losses of 2% and 31% which may be due to the loss of adsorbed water. The DTG patterns also show the thermal stability of the samples up to 1400 K.

The FTIR patterns of $MgAl_2O_4$ and of $Mg_{0.2}Zn_{0.4}Ni_{0.4}Al_2O_4$ are shown in Fig. 5. The formation of spinel is confirmed by the appearance in the FTIR patterns of the peaks at 550 and 712 cm^{-1} due to metal-oxygen stretching due to vibration of MO–Al–O and M–O–Al bonds respectively, which are characteristic for spinel [26]. The peaks at 3505 and 1763 cm^{-1} are due to O–H and C=O stretches caused by moisture and CO_2 adsorbed from the air during the pressing of pellets.

The electrical resistivity of these materials follows the Arrhenius type equation given below, with resistivity decreasing exponentially on increasing temperature:

$$\rho = \rho_0 \exp\left(\frac{E}{k_b T}\right) \quad (4)$$

The resistivity behavior in the range of T = 298–673 K for $MgAl_2O_4$ and for a series of doped samples ($Mg_{1-2x}Zn_xNi_xAl_2O_4$) where x = 0.1–0.5 are shown in Fig. 6. A maximum in the resistivity curves is observed at a temperature of about 400 K which is due to adsorbed moisture and CO_2 because magnesium aluminate is known for its moisture sensitive nature [27] The peaks in the FTIR patterns at 3200–3500 and 1690–1760 cm^{-1} also point towards the above conclusion. The activation energy (E) is calculated from the

Table 1
Characteristics of $Mg_{1-2x}Zn_xNi_xAl_2O_4$ (x = 0.0–0.5) samples.

	$Mg_{1-2x}Ni_xZn_xAl_2O_4$					
	0.0	0.1	0.2	0.3	0.4	0.5
Lattice parameter, a (Å) ± 0.02	8.07	8.10	8.08	8.07	8.10	8.06
Cell volume, V_{cell} (Å^3) ± 5	526	531	528	526	531	524
Density, $d_{X\text{-ray}}$ (g/cm^3) ± 0.01	3.60	3.80	4.10	4.16	4.23	4.56
Scherrer crystallite size, D (nm) ± 5	42	26	51	31	28	24
Resistivity, ρ (Ω cm) × 10^9 ± 1.45 (RT)	0.27	7.62	8.84	9.41	1.08	1.19
Resistivity, ρ (Ω cm) × 10^8 ± 1.45 (623 K)	0.83	5.67	4.27	3.83	3.57	3.52
Activation energy, E (eV) ± 0.15	0.65	0.55	0.54	0.63	0.49	0.53
Dielectric constant, ε ± 0.01 (10 kHz)	2.97	40.67	10.02	5.56	6.66	22.49
Dielectric constant, $\hat{\varepsilon}$ ± 0.01 (100 kHz)	0.40	15.21	5.93	3.88	4.90	11.52
Dielectric constant, $\hat{\varepsilon}$ ± 0.01 (1000 kHz)	0.37	7.10	3.99	3.31	4.19	8.26
Loss tangent, tan δ ± 0.0001 (1000 kHz)	0.0035	0.2800	0.0700	0.0061	0.0362	0.1400
Al (mol)	2.08	1.80	1.90	1.78	1.91	1.85
Mg (mol)	0.90	0.72	0.58	0.37	0.18	–
Ni (mol)	–	0.09	0.18	0.27	0.39	0.47
Zn (mol)	–	0.07	0.16	0.25	0.35	0.42

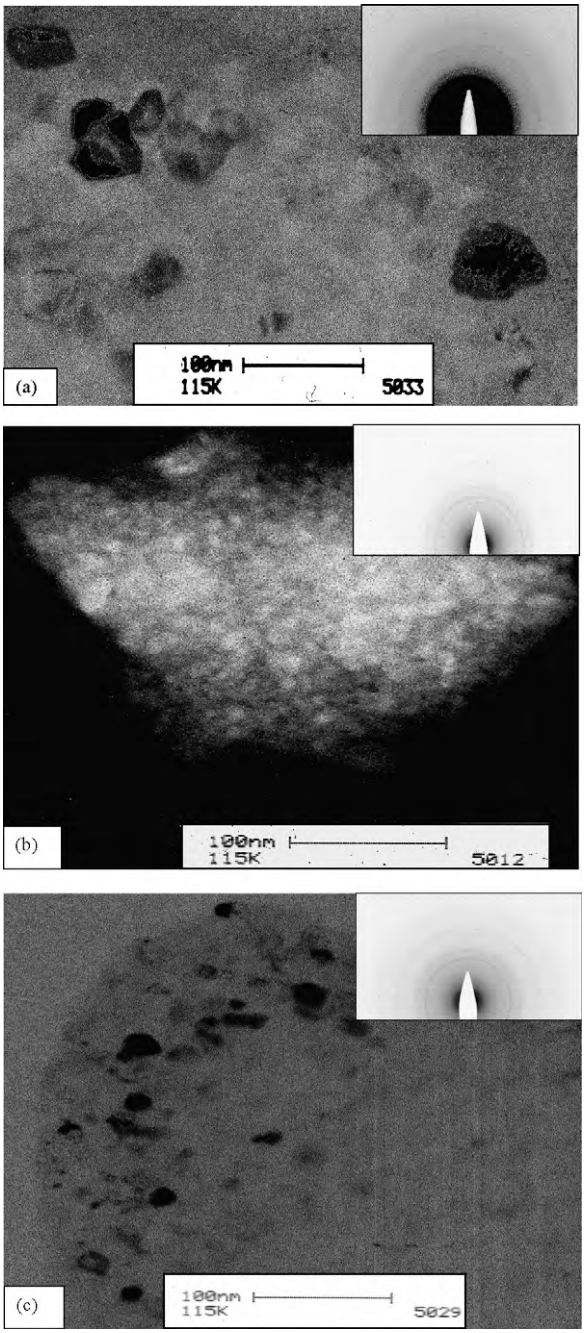

Fig. 3. HRTEM images of the samples (a) $MgAl_2O_4$, (b) $Mg_{0.6}Ni_{0.2}Zn_{0.2}Al_2O_4$, and (c) $Mg_{0.2}Ni_{0.4}Zn_{0.4}Al_2O_4$.

slope of the plot of ln ρ versus $10^3/T$ according to Eq. (4) as shown in Fig. 7 and varies in the range of 0.49–0.65 eV as listed in Table 1.

The decreasing resistivity with an increase in temperature validates the small-polaron hopping conduction mechanism in the samples. Synthetic magnesium aluminate is normally a partially inverse spinel owing to cationic disorder in the structure of the spinel. It leads to the formation of charged anti-site defects, electron–hole (Al^{3+} in A-site) and traps (Mg^{2+} in B-site), which are responsible for the hopping of electrons in the structure of the ceramic $MgAl_2O_4$ material [18]. The hopping takes place through interstitial sites for the occupancy of Al^{3+} and Mg^{2+} ions in the octahedral sites. The transfer of charge carriers between adjacent Mg^{2+} ions takes place via O^{2-} ions present in the spinel system. The hopping of an electron between adjacent sites results in a local

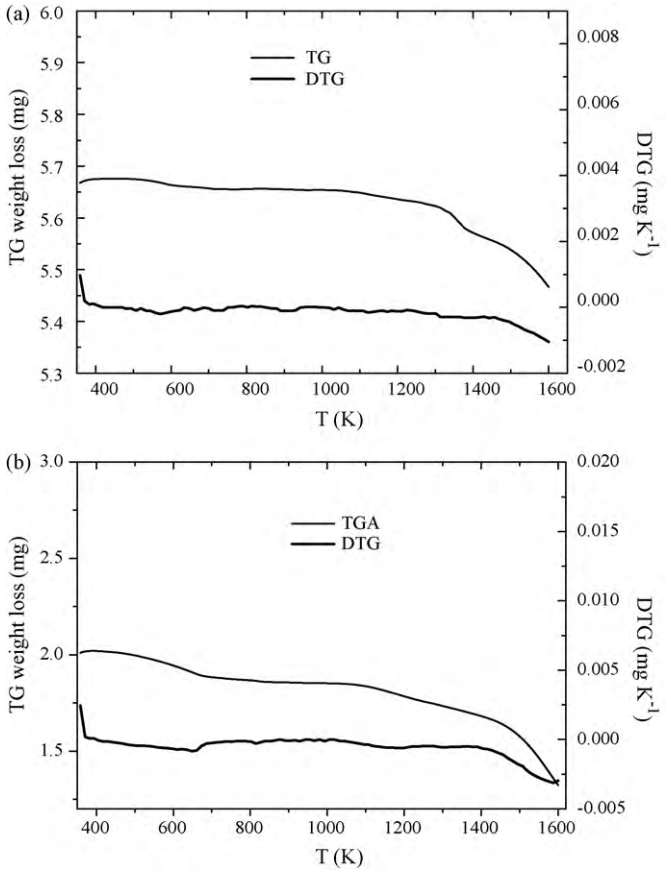

Fig. 4. TG/DTG patterns for (a) $MgAl_2O_4$ and (b) $Mg_{0.2}Zn_{0.4}Ni_{0.4}Al_2O_4$.

displacement in the direction of an applied local electric field and a vacancy is created due to the hopping. Therefore, the charge carriers are either localized at the ions (Mg^{2+}, Al^{3+}) or at the vacant sites that take part in the conduction process via the hopping-type process [18].

Values of resistivity at room temperature and at 623 K are given in Table 1. The resistivity of magnesium aluminate at room temperature is $0.27 \times 10^9\ \Omega$ cm, as magnesium aluminate is known as a hopping semiconductor in which energy is required for the mobility of charge carriers. A considerable extent of cation inversion may occur in the synthetic samples prepared at high temperatures, and Mg^{2+} and Al^{3+} may exchange their respective sites that is responsible for the low conductivity of the samples has a high activation

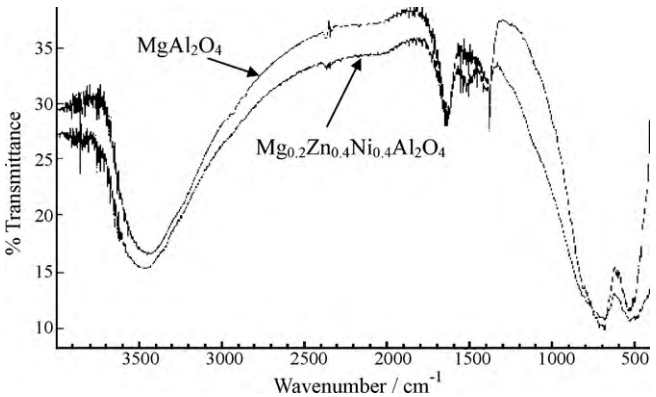

Fig. 5. Comparison of FTIR patterns for samples of $MgAl_2O_4$ and $Mg_{0.2}Zn_{0.4}Ni_{0.4}Al_2O_4$.

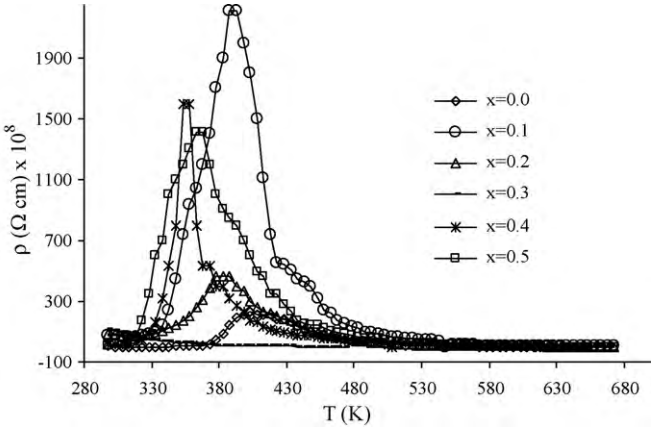

Fig. 6. Comparison of resistivity profiles for samples of $Mg_{1-2x}Ni_xZn_xAl_2O_4$ containing different Ni_xZn_x contents, i.e. $x = 0.0–0.5$.

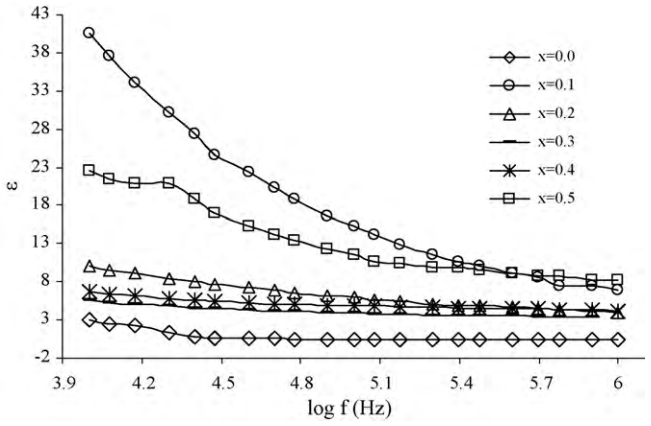

Fig. 8. Profiles of dielectric constant (ε) against frequency for a series of $Mg_{1-2x}Ni_xZn_xAl_2O_4$ samples where $x = 0.0–0.5$.

energy of hopping (0.65 eV) is required. A remarkable increase in the resistivity values, i.e. from 0.83×10^8 to $5.67 \times 10^8\ \Omega$ cm (at 623 K) is observed by doping with Ni/Zn. Due to the strong octahedral site preference of Ni^{2+} ions [28], some of the Al^{3+} ions move to tetrahedral sites resulting in the creation of more 'hole' traps in the lattice, hence enhancing the values of resistivity on doping.

Increasing the dopant content has an effect on the resistivity of the Ni/Zn samples which decreases with an increase in the content as shown in Table 1 for a temperature of 623 K. The loss of Zn during synthesis of the samples forms cation vacancies [25], and to maintain the charge balance some of the Ni^{2+} would be converted to Ni^{3+}. Due to the 'hole' formation, a decrease in resistivity with enhanced doping is observed at the octahedral sites.

The dielectric constant (ε) and the loss factor ($\tan\delta$) are measured as a function of frequency in the range of 1 kHz to 1 MHz. The dielectric constant (ε) is calculated by the following relation:

$$\varepsilon = \frac{C \cdot d}{\varepsilon_o A} \tag{5}$$

where C is the capacitance of the pellet, d and A are the thickness and the cross-sectional area of the flat surface of the pellet, respectively, and ε_o is the permittivity constant of free space. The dielectric loss factor ($\tan\delta$), also called dissipation factor, is the ratio of the power loss in a dielectric material to the total power transmitted through the dielectric, and it is calculated from the following equation:

$$\tan\delta = \frac{1}{2\pi f C_p R_p} \tag{6}$$

where δ is the loss angle, f is the frequency, R_p is the equivalent parallel resistance, and C_p is the equivalent parallel capacitance.

Plots of ε and $\tan\delta$ are shown in Figs. 8 and 9, respectively, and the values of ε at 10, 100 and 1000 kHz, and of $\tan\delta$ at 1000 kHz are given in Table 1. The value of ε decreases with an increase in the applied frequency (Fig. 8) and becomes eventually constant at higher frequencies. The higher values of the dielectric constant at lower frequencies are due to voids, dislocations and other defects [29] in single crystals; in powdered samples the polarization processes decreases at the higher frequencies as the dipoles cannot follow the fast reversal of the applied electric field. The dielectric structure is supposed to be composed of highly conducting grains separated by relatively poorly conducting grain boundaries [30]. This causes the localized accumulation of charges under the influence of an electric field resulting in the interfacial polarization. The $\tan\delta$ also decreases with the frequency (Fig. 9).

The grain boundaries are active at lower frequencies and the grains at the higher frequencies. At lower frequencies more energy is required for the polarization in the grain boundaries, thus energy loss is high, while at high-frequencies a small energy is required for polarization in the grains, and hence the energy loss is small. The low values of both the dissipation factor and dielectric constant as well as higher values of the resistivity favor the use of these materials in the electronic materials industry.

In Table 2, a comparison of different properties of the synthesized zinc aluminate spinel, nickel aluminate spinel, magnesium

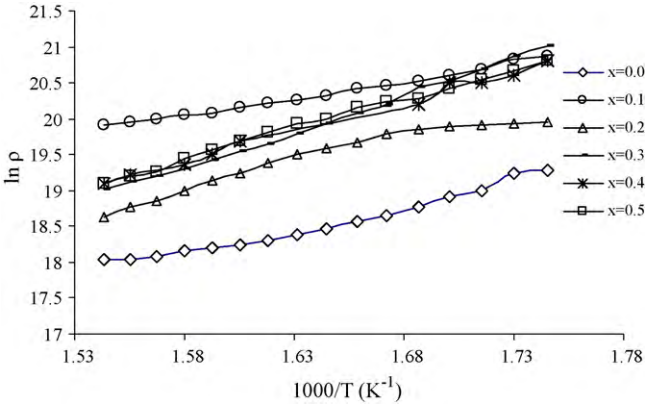

Fig. 7. Arrhenius type plots of $\ln\rho$ against temperature as $1000/T$ for the $Mg_{1-2x}Ni_xZn_xAl_2O_4$ where $x = 0.0–0.5$.

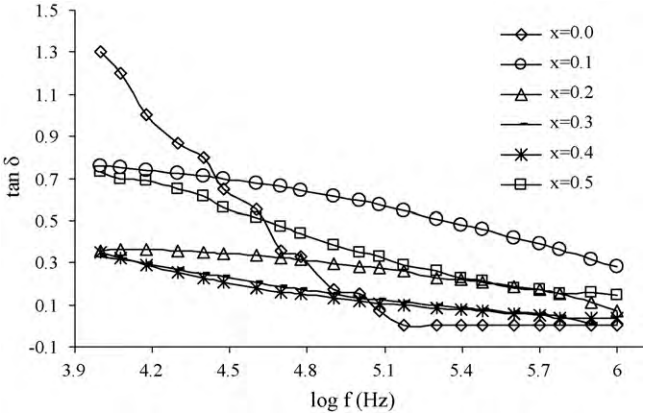

Fig. 9. Profiles of dissipation factor ($\tan\delta$) against frequency for the synthesized $Mg_{1-2x}Ni_xZn_xAl_2O_4$ samples where $x = 0.0–0.5$.

Table 2
Comparison of various properties of the doped and undoped spinel magnesium aluminate.

	D (nm)	a (Å)	V_{cell} (Å^3)	$d_{X\text{-ray}}$ (g/cm^3)	ρ (nΩ cm) (673 K)	ε (1 MHz)	$\tan\delta$ (1 MHz)
Sol–gel synthesized [20]	6	8.10	531	3.62	0.20	9.99	0.09
Modified sol–gel synthesized [20]	13	8.20	533	3.50	0.34	10.94	0.09
Coppt. with NH_3 at pH 9 [18]	13	8.10	531	3.54	0.07	8.09	0.11
Microwave combustion (present study)	42	8.07	526	3.60	0.27	0.37	0.0035
Conventional combustion [19]	19	8.10	531	3.56	3.09	5.80	0.0051
$ZnAl_2O_4$ (present study)	11	8.09	529	4.64	0.16	6.96	0.295
$NiAl_2O_4$ (present study)	11	8.09	531	4.40	0.32	5.02	0.55
$Mg_{0.8}(Ni, Zn)_{0.1}Al_2O_4$ (present study)	26	8.10	531	3.80	7.62	7.10	0.28
$MgAl_{1.92}(Zr, Co)_{0.04}O_4$ [19]	14	8.11	533	3.64	4.45	5.62	0.003
$MgAl_{1.92}(Zr, Ni)_{0.04}O_4$ [19]	8	8.02	516	3.75	4.61	5.57	0.003

aluminate spinel and doped samples is presented. The dielectric constant and the dielectric loss values determined at 1 MHz for the microwave synthesized samples are 0.37 and 0.0035, respectively, which are lower than the values for spinel materials synthesized reported previously by a urea assisted conventional combustion method ($\varepsilon = 5.80$, $\tan\delta = 0.0051$) [19] and by a co-precipitation method ($\varepsilon = 8.09$, $\tan\delta = 0.11$ at pH 9) [18]. Similarly, the room temperature resistivity values for samples in which Zr/Ni and Zr/Co were doped at octahedral sites of magnesium aluminate spinel [19] vary as $3.25–6.45 \times 10^9$ and $3.14–6.73 \times 10^9$ Ω cm, respectively. For the present samples the corresponding values are $1.19–9.41 \times 10^9$ Ω cm. A better optimization of electrical resistivity, dielectric constant and dielectric loss is achieved by co-doping Zn/Ni on the magnesium aluminate lattice (Table 2).

The random behavior of different properties with increasing concentration of dopants (Tables 1 and 2) is due to the fact that the site occupation of ions in the lattice varies randomly as spinels synthesized at high temperatures are found to have anti-site defects [31] causing cationic disorders which effect the properties of spinel even though the concentration of dopants is varied continually. The synthesis methods also influence properties of the synthesized materials [32]. Porosity in the samples (Figs. 2 and 3) may also result in a similar variation of the properties.

4. Conclusions

A urea assisted microwave combustion technique was used to synthesize magnesium aluminate and its doped derivatives $Mg_{1-2x}Zn_xNi_xAl_2O_4$ where $x = 0.1–0.5$. This method was found more energy efficient than the conventional methods due to the shorter reaction time. Well-crystallized single-phase spinels were evident from XRD patterns with lattice constant and cell volume matching the standard spinel pattern. The Scherrer crystallite size was measured to be in the range of 24–51 nm and was confirmed by TEM analysis. High values of resistivity ($0.27–9.41 \times 10^9$ Ω cm at room temperature) combined with resistivity-temperature profiles in the range of 298–673 K show that the synthesized materials behave as semiconductors. The double Ni/Zn doped samples have a higher value of resistivity ($3.52–5.67 \times 10^8$ Ω cm at 673 K) than the undoped magnesium aluminate 0.83×10^8 Ω cm in the same temperature. The resistivity decreases with an increase in Ni/Zn content. The values of both the dissipation factor and the dielectric constant decrease with an increase in frequency. These observations are consistent with active grain boundaries at lower frequencies and active grains at higher frequencies.

Acknowledgements

This work has been supported by the Indigenous 5000 Scholarship Scheme and International Research Support Initiative Program (IRSIP) of the Higher Education Commission (HEC) of Pakistan. We are also thankful to Prof. Dr. Shahzad Naseem (Centre of Excellence in Solid State Physics, University of the Punjab, Lahore, Pakistan) for providing SEM facility and Prof. Dr. Herbert Ipser (Department for Inorganic Chemistry/Materials Chemistry, University of Vienna, Austria) for coordinating research with Prof. Dr. Christian Rentenberger (Physics of Nanostructured Materials, University of Vienna, Austria) at the TEM facility.

References

[1] E.N. Alvar, M. Rezaei, H.N. Alvar, Powder Technol. 198 (2010) 275–278.
[2] A. Saberi, F.G. Fard, M.W. Porada, Z. Negahdari, C. Liebscher, B. Gossler, Ceram. Int. 35 (2009) 933–937.
[3] F. Tavangarian, R. Emadi, J. Alloys Compd. 489 (2010) 600–604.
[4] I. Ganesh, G.J. Reddy, G. Sundararajan, S.M. Olhero, P.M.C. Torres, J.M.F. Ferreira, Ceram. Int. 36 (2010) 473–482.
[5] A. Mussi, G.B. Granger, A. Addad, N. Benameur, F. Beclina, A. Bataille, Scr. Mater. 61 (2009) 516–519.
[6] E.N. Alvar, M. Rezaei, Scr. Mater. 61 (2009) 212–215.
[7] L. Henkel, D. Koch, G. Grathwohl, J. Am. Ceram. Soc. 92 (2009) 805–811.
[8] J. Chandradass, M. Balasubramanian, D.S. Bae, J. Kim, K.H. Kim, J. Alloys Compd. 491 (2010) L24–L28.
[9] R.J. Wiglusz, T. Grzyb, S. Lis, W. Strek, J. Lumin. 130 (2010) 434–441.
[10] A. Troia, M. Pavese, F. Geobaldo, Ultrason. Sonochem. 16 (2009) 136–140.
[11] L. Torkian, M.M. Amini, Z. Bahrami, J. Surf. Sci. Nanotechnol. 8 (2010) 112–114.
[12] L. Ma, L.M. Xu, W.X. Chen, Z.D. Xu, Mater. Lett. 63 (2009) 1635–1637.
[13] J. Lin, Y. Huang, J. Zhang, F. Shi, S. Wei, J. Gao, X. Ding, C. Tang, Mater. Res. Bull. 44 (2009) 106–109.
[14] I. Omkaram, B.V. Rao, S. Buddhudu, J. Alloys Compd. 474 (2009) 565–568.
[15] I. Omkaram, S. Buddhudu, Opt. Mater. 32 (2009) 8–11.
[16] H. Pan, R. Li, Y. Liu, M. Gao, H. Miao, Y. Lei, Q. Wang, J. Alloys Compd. 463 (2008) 189–195.
[17] P. Głuchowski, R. Pazik, D. Hreniak, W. Strek, Chem. Phys. 358 (2009) 52–56.
[18] M.J. Iqbal, B. Ismail, J. Alloys Compd. 472 (2009) 434–440.
[19] M.J. Iqbal, B. Kishwar, Mater. Res. Bull. 44 (2008) 753–758.
[20] M.J. Iqbal, S. Farooq, Mater. Sci. Eng. B 136 (2007) 140–147.
[21] B.M. Reddy, G.K. Reddy, A. Khan, I. Ganesh, J. Mater. Sci. 42 (2007) 3557–3563.
[22] A. Saberi, F. Golestani-Fard, H. Sarpoolaky, M. Willert-Porada, T. Gerdes, R. Simon, J. Alloys Compd. 462 (2008) 142–146.
[23] R. Ianos, R. Lazau, Mater. Chem. Phys. 115 (2009) 645–648.
[24] B.D. Cullity, Elements of X-ray Diffraction, Addison-Wesley, London, 1956.
[25] I.H. Gul, W. Ahmed, A. Maqsood, J. Magn. Magn. Mater. 320 (2008) 270–275.
[26] C. Wang, S. Liu, L. Liu, X. Bai, Mater. Chem. Phys. 96 (2006) 361–370.
[27] G.D. Bromiley, F. Nestola, S.A.T. Redfern, M. Zhang, Geochim. Cosmochim. Acta 74 (2010) 705–718.
[28] A. Navrotsky, O.J. Kleppa, J. Inorg. Nucl. Chem. 29 (1967) 2701–2714.
[29] L. Sirdeshmukh, K. Kumar, B. Laxman, K.A. Rama, G. Sathaiah, Bull. Mater. Sci. 21 (1998) 219–226.
[30] R.V. Mangalaraja, S. Ananthakumar, P. Manohar, J. Magn. Magn. Mater. 253 (2002) 56–64.
[31] V.T. Gritsyna, I.V. Afanasyev-Charkin, Y.G. Kazarinov, K.E. Sickafus, Vacuum 81 (2006) 174–178.
[32] M.J. Iqbal, M.N. Ashiq, Scr. Mater. 56 (2007) 145–148.